Recent Refinements in Geophysical Constraints on Lunar Origin and Evolution

Lon L. Hood
University of Arizona

Maria T. Zuber
Massachussetts Institute of Technology

Recent, more complete geophysical mapping of the Moon by the Clementine and Lunar Prospector missions, as well as continued analysis and interpretation of the Apollo lunar seismic dataset, have significantly improved existing geophysical constraints on lunar origin and evolution. Gravity and topography data indicate large lateral variations in crustal thickness (~20–110 km) and a range of compensation states that imply a more complex near-surface thermal history than had previously been considered. A recent P-wave mantle velocity model together with earlier quantitative modeling strongly suggests that initial melting and differentiation of the lunar interior was limited to depths <500 km. Recent analyses of Lunar Prospector magnetometer, gravity, and groundbased laser-ranging data strengthen earlier conclusions that the Moon most probably possesses a metallic core with a mass of 1–3% of the lunar mass.

1. INTRODUCTION

Geophysical observations impose quantitative constraints on the internal structure, thermal state, thermal history, and bulk composition of the Moon. Gravity and topography data can, with reasonable assumptions, be applied to estimate crustal thickness and its lateral variability on a global scale. These data can also be applied to assess the rigidity of the lithosphere as a function of time during lunar evolution. Seismic data impose quantitative constraints on crustal structure beneath the Apollo landing sites and on mantle structure, thermal state, and composition as a function of depth. Gravity (moment of inertia), electromagnetic sounding, and laser ranging data together impose significant constraints on the existence and size of a possible metallic core. These results can, in turn, be applied to address several fundamental issues that are relevant to lunar origin and evolution, including (1) the early thermal state and lateral heterogeneity of the lunar lithosphere, (2) the bulk composition of the crust and mantle, (3) the depth of initial melting and differentiation, and (4) the bulk lunar metallic Fe content.

Previous reviews by *Hood* (1986) (hereinafter *H86*) and *Solomon* (1986) have summarized geophysical constraints derived from Apollo-era measurements on lunar origin and early evolution. Since that time, a series of developments has led to significant refinements of these constraints. First, several comprehensive assessments and syntheses of available geophysical and petrological constraints on lunar bulk composition have been reported (*Hood and Jones*, 1987; *Mueller et al.*, 1988). These analyses were stimulated, in part, by a more accurate seismic velocity model of the lunar mantle (*Nakamura*, 1983), based on the complete five-year Apollo dataset. In addition, *Khan et al.* (2000) have recently derived an improved P-wave mantle velocity model using more advanced computational resources than were available during the immediate post-Apollo period. Second, more complete orbital geophysical measurements have recently been acquired by instruments onboard the Clementine and Lunar Prospector spacecraft (*Nozette et al.*, 1994; *Binder et al.*, 1998). These new analyses and measurements have led to notable refinements of geophysical constraints on lunar origin and evolution. In this chapter, these refined constraints are reviewed. In section 2, improved analyses of topography and gravity data with implications for near-surface structure and evolution are summarized. In section 3, the interpretation of mantle seismic velocity models is reviewed with emphasis on implications for bulk composition and depth of initial melting and differentiation. In section 4, a brief review is presented of geophysical constraints on the existence and size of a metallic core, including several recent results based on Lunar Prospector data. In section 5, a summary of those results that are most relevant to lunar origin and evolution models is given.

2. NEAR-SURFACE STRUCTURE AND THERMAL STATE

Observations from topography and gravity have provided useful information regarding lunar internal structure. When the gravitational attraction of surface topography is removed from the gravity field, the remaining (Bouguer) gravity represents the distribution of density anomalies in the interior that are indicative of lateral variations in composition and/or thermal state. However, gravity/topography inversions are

inherently nonunique and benefit from independent geophysical (mainly seismic) and geochemical constraints. Topography and gravity can be used to address the rigidity of the lunar lithosphere at the time of loading by surface topography or subsurface density variations and provide evidence for early rigidity of the lunar lithosphere. Certain aspects of the long-wavelength lunar shape may also preserve the record of rigidity in the outer parts of the Moon early in its evolution.

The first high-quality lunar topography was obtained from laser altimetry on Apollos 15, 16, and 17 (e.g., *Kaula et al.,* 1974). A total of 7080 range measurements was collected from the three missions and these measurements, when converted to lunar radii by correcting for the orbit of the spacecraft, provided the first information on the shape of the Moon in a geodetic, center-of-mass reference frame. The along-track sampling of the measurements was 30–43 km, and the vertical resolution was ~12 m. The absolute radial accuracy of the measurements, which was controlled by radial orbit knowledge of the Apollo Command and Service Modules, was ~400 m. In addition, a radar sounder experiment on Apollo 17 acquired essentially continuous data along the orbit track but had lower vertical resolution (*Brown et al.,* 1974). The greatest limitation of the Apollo altimeter data was the coverage, which was restricted to within 26° of the equator. However, these data provided a measure of the Moon's equatorial radius and in addition led to the identification of the ~2.55-km offset between the Moon's center of figure and center of mass (*Kaula et al.,* 1974).

Prior to the Clementine Mission (sponsored by the Ballistic Missile Defense Organization and NASA; *Nozette et al.,* 1994), the best global-scale representation of lunar topography was a 12th degree and order spherical harmonic model by *Bills and Ferrari* (1977) that incorporated Apollo laser altimeter data, orbital photogrammetry and landmark measurements, and limb profiles. The estimated error for individual data types in that model ranged from 300 to 900 m; however, vast regions on the lunar farside lacked any measured topography. Near-global topography obtained from the Clementine lidar (*Zuber et al.,* 1994; *Smith et al.,* 1997) precipitated a significant advance in characterizing the structure of the lunar interior. The best current representation of the shape of the Moon is shown in Fig. 1a. The field is Goddard Lunar Topography Model-2 (GLTM-2), a 72nd degree and order spherical harmonic expansion of lunar radii derived from the ~73,000 valid Clementine lidar range measurements. The GLTM-2 model has an absolute vertical accuracy of ~100 m and a spatial resolution of 2.5° (76 km at the equator). The model shows that the Moon can be represented as a sphere with maximum positive and negative deviations of ~8 km, both occurring on the farside, in the areas of the Korolev and South Pole-Aitken Basins. The amplitude spectrum of the topography field exhibits significantly more power at longer wavelengths as compared to previous models due to more complete sampling of the lunar surface, particularly on the farside in areas of large topographic variance. The mechanism of support for this topography has implications for the Moon's internal structure and geodynamical evolution.

Gravity models of the Moon have been developed from S- and X-band Doppler tracking of orbiting spacecraft, principally the Lunar Orbiters, Apollo Command modules and subsatellites, and the Clementine and Lunar Prospector spacecraft. The Lunar Orbiters were typically in elliptical orbits with periapses of 50–100 km above the lunar surface, while the Apollo spacecraft occupied near-circular orbits at low inclinations with a mean altitude of 100 km, although via the subsatellites on Apollos 15 and 16 some tracking was acquired from altitudes as low as 10–20 km. Clementine occupied a polar elliptical orbit with a periapsis altitude of 400 km. Lunar Prospector spent its first year in an ~100-km altitude circular polar orbit, but the orbit altitude was lowered to a mean of ~30 km for the final seven months of the mission.

Earliest lunar gravity analyses utilized differentiated Doppler residuals, which correspond to the signal that remains after numerical integration of the equations of motion and correction for all forces on the spacecraft, including the gravitational attraction of Earth, the Sun, and the other planets, radiation pressure, and relativistic effects. During the Apollo era only the Moon's central mass term was accounted for, so the residuals contained the total resolvable information on the lunar gravity field (*Phillips et al.,* 1978). Doppler-derived accelerations are in the line of sight between spacecraft and radio tracking stations on Earth and thus necessarily sample the vertical component of gravity in a nonuniform manner over the surface. Analysis of line-of-sight gravity led to the discovery of the lunar mass concentrations (mascons) over the nearside maria (*Muller and Sjogren,* 1968). Subsequent spherical harmonic solutions based on Doppler observations from multiple satellites (*Bills and Ferrari,* 1980) combined pre-Clementine spacecraft tracking data with Earth-based lunar laser ranging observations to produce a 16th degree and order spherical harmonic solution (340-km half-wavelength resolution). *Konopliv et al.* (1993) produced the first high-resolution spherical harmonic model from the tracking of the Lunar Orbiters and Apollo subsatellites. This 60th degree and order expansion exhibited excellent performance in terms of orbit prediction but contained short wavelength noise that made it nonoptimal for regional scale geophysical studies. Clementine gravity models (*Zuber et al.,* 1994; *Lemoine et al.,* 1997) with a maximum resolution of 70th degree and order were characterized by improved short-wavelength control to enable basin modeling, and in addition provided improved knowledge of the low-degree harmonics and sectorial terms of the lunar field. The combination of tracking observations from Lunar Prospector with historical observations yielded a 75th degree and order field (*Konopliv et al.,* 1998), shown in Fig. 1b, as well as a very recent 100th degree and order field (A. Konopliv, personal communication, 1999) with a half-wavelength resolution of 55 km where the data permit. Compared to Clementine models, the Lunar Prospector gravity fields are characterized by better long-wavelength control and improved short-wavelength

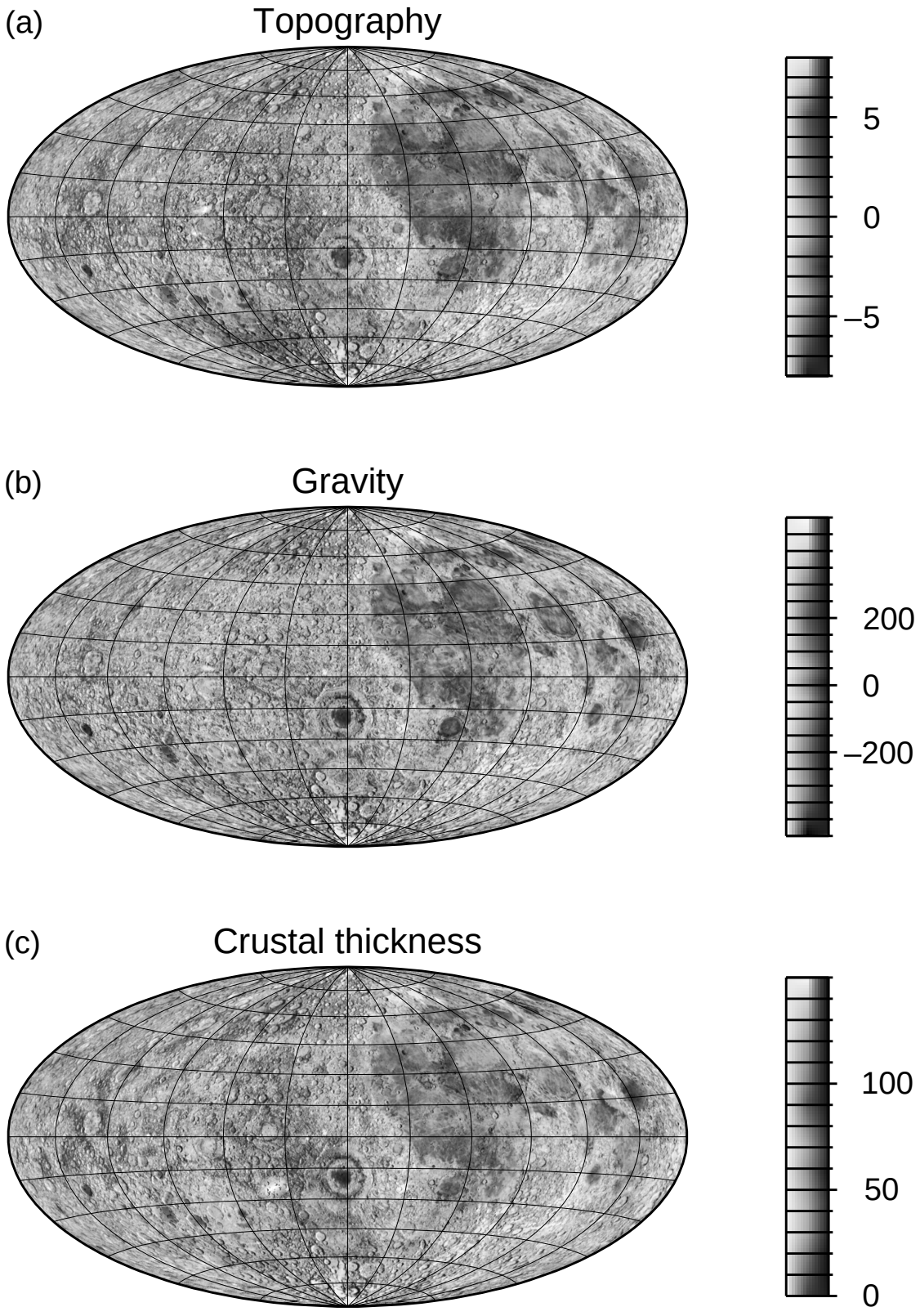

Fig. 1. Lunar topography, gravity, and crustal thickness. **(a)** Topography model GLGM-2 (*Smith et al.*, 1997). **(b)** Gravity model LP75G (*Konopliv et al.*, 1998). **(c)** Single-layer Airy compensation crustal thickness model updated from *Wieczorek and Phillips* (1998) using topography model GLTM-2 and gravity model LP75D.

resolution, the latter of which is facilitating more detailed regional modeling of nearside basins.

Despite the global nature of spherical harmonic solutions, all the gravitational models produced thus far are plagued by a lack of direct tracking on the lunar farside. Because the spacecraft is sensitive to perturbations of a range of wavelengths, some information on the spatial distribution of lunar farside gravity is obtained from spacecraft orbital changes as spacecraft enter and exit occultation, even when the spacecraft is not directly above features of interest. However, the magnitudes of anomalies are unreliable and thus cannot be used for geophysical modeling.

The thickness of the lunar crust provides an indication of the extent of melting of the lunar exterior in its early history. Crustal thickness has traditionally been determined by modeling the lunar gravity and topography fields. Given simplifying assumptions (cf. *Solomon,* 1978; *Thurber and Solomon,* 1978) including the densities and possible lateral variations of density in the crust and mantle, as well as the mode of compensation, Bouguer gravity can be converted to crustal thickness. Published crustal thickness models differ in detail, but all are "anchored" by the seismically determined crustal structure beneath the Apollo 12 and 14 sites. An early inversion (*Bratt et al.,* 1985) captured essential features such as the nearside-farside crustal thickness difference and the thinning of the crust beneath major impact basins, but that analysis was limited by the absence of reliable, near-global topography.

A common feature of the Clementine and Lunar Prospector gravity models is that highland regions are characterized by low-amplitude anomalies that reflect a state of isostatic compensation of surface topography. In principle, such compensation may be achieved either by an Airy mechanism (thickness variations of a constant-density crust) or by a Pratt mechanism (lateral density variations within a constant-thickness crust or in the upper mantle), or by some combination of the two. Evidence against a significant component of Pratt compensation has been presented, for example, by *Wieczorek and Phillips* (1997, their Fig. 8) based on a near lack of correlation of surface Fe abundance with elevation for the nearside highlands. Crustal thickness models based on near-global Clementine topography combined with the gravity models (*Zuber et al.,* 1994; *Neumann et al.,* 1996; *Solomon and Simons,* 1996; *Wieczorek and Phillips,* 1998) have therefore most commonly assumed compensation of topography by an Airy mechanism that assumes a strengthless lunar lithosphere in which pressures in vertical columns are balanced by relief along a single subsurface interface. Such models show a large range of global crustal thickness (~20–110 km) that would require major spatial variations in melting of the lunar exterior and/or significant impact-related redistribution of lunar crust (*Zuber et al.,* 1994). The ~61-km average crustal thickness, constrained by a depth-to-Moho measured during the Apollo 12 and 14 missions, is preferentially distributed toward the farside, accounting for much of the offset in center-of-figure from the center-of-mass (*Kaula et al.,* 1974). While the average farside crustal thickness is greater than that on the nearside, the distribution is nonuniform. Most significantly, the South Pole-Aitken Basin on the lunar farside is an extensive region of crust that is much thinner than the nearside average. In Airy models the anorthositic lunar crust comprises ~10% of the volume of the Moon. Global multispectral observations show the interior of the South Pole-Aitken Basin to be more mafic than its surroundings (*Lucey et al.,* 1994, 1998), which would suggest internal compositional layering. The nature of such layering has been explored in crustal thickness inversions by *Wieczorek and Phillips* (1997, 1998), who demonstrated the viability of an internal structure with two crustal layers. Future attempts to refine shallow compositional structure from crustal thickness models will require incorporation of geochemical information, particularly in areas surrounding impact basins that have excavated deeply into the crust and reveal the shallow subsurface structure.

On a regional scale, the crustal structure in the vicinity of major impact structures has been recently improved. Gravity data show that nearside and some farside basins are characterized by strong positive mascon anomalies often surrounded by negative rings that represent subsurface mass deficiencies (*Muller and Sjogren,* 1968; *Zuber et al.,* 1974). Recent geophysical prospecting has revealed that these negative rings also characterize the Chicxulub basin on Earth and major impact basins on Mars (*Smith et al.,* 1999) and are thus fundamental features of impact basins. Modeling studies that incorporate recent estimates of mare fill thickness (*Williams and Zuber,* 1998; *Budney and Lucey,* 1998) show that the mascons are a consequence of a combination of mare filling and uplifted crust associated with rebound that occurred as part of the impact process (*Wise and Yates,* 1970; *Phillips and Dvorak,* 1981; *Melosh,* 1989). It follows that a mascon can, in principle, be produced without any mare fill (*Phillips and Dvorak,* 1981) and several such structures have recently been resolved on the farside from Lunar Prospector gravity fields (*Konopliv et al.,* 1998). Figure 2 illustrates the inferred subsurface structure via an inversion for crustal structure beneath the Orientale Basin. Surrounding the thinned central region is an apparent ring of thickened crust. While brecciation or comminution of crustal material associated with the impact process has been invoked to explain these features (*von Frese et al.,* 1996), such effects cannot in themselves plausibly account for the magnitudes of the observed mass deficiencies.

On the basis of elastic plate models constrained by observed tectonic features, it has been realized for some time that the lunar lithosphere exhibited demonstrable rigidity at the time of mare loading (e.g., *Comer et al.,* 1979; *Solomon and Head,* 1980). Clementine and Lunar Prospector observations now indicate that the lithosphere was strong enough to support loads even earlier in lunar history. In regional models of the subsurface structure of some mare basins, local isostatic models cannot fit the gravity data and it appears that relief at the surface and along the Moho was

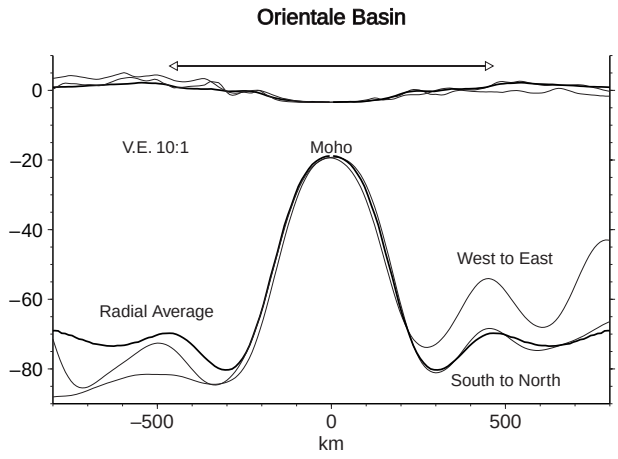

Fig. 2. West to east, south to north, radial average profiles of surface topography and Moho depth from an inversion using the method of *Neumann et al.* (1996) using GLTM-2 and LP75G. The model assumed a 1.7-km-thick mare load and an average depth to Moho as determined by *Wieczorek and Phillips* (1997).

supported by the strength of the lithosphere prior to mare filling (*Zuber et al.,* 1994). For example, the data for Orientale (Fig. 2) indicates that if this basin was isostatic before mare emplacement, then more than 5 km of mare fill would be required to account for the observed gravity field. Such a value is implausible since in this basin the maximum mare fill thickness is well-constrained to be less than 2 km (*Solomon and Head,* 1980; *Williams and Zuber,* 1998). Both the central uplift beneath the basin and the surrounding depression of the Moho are nonisostatic effects indicative of early lithospheric rigidity. *Neumann et al.* (1996) have identified a negative correlation between Moho relief and age, which indicates that basins formed at later times maintained a greater amount of the uplift resulting from the impact process. This observation provides qualitative evidence for cooling and thickening of the outer shell of the early Moon.

Additional evidence for early lunar rigidity comes from the Moon's long-wavelength shape. The present topographic shape of the Moon is flattened by 2.2 km, while its gravity field is flattened only ~0.5 km (*Smith and Zuber,* 1998). The hydrostatic component of the flattening, i.e., that which arises from the Moon's present-day rotation, is only 7 m. This difference between the topographic and gravitational equipotential shape has previously been explained as the "memory" of an earlier Moon that was rotating faster and had a correspondingly larger hydrostatic flattening (*Jeffreys,* 1970; *Lambeck and Pullan,* 1980; *Willemann and Turcotte,* 1981). Recent analysis (*Smith and Zuber,* 1998) has shown that other degree-2 terms of the lunar topographic field also exceed significantly their counterparts in the gravity field (*Konopliv et al.,* 1998) and are mutually consistent with a lunar rotation rate about 15× greater than at present. Assuming synchronous rotation, the degree-2 topography would require that the Moon "froze in" its long-wavelength shape at a distance of 13 to 16 Earth radii. Such a scenario is problematic given dynamical studies (e.g., *Goldreich,* 1966; *Touma,* 2000) of the evolution of the Earth-Moon system that suggest that the Moon, which had a mostly molten exterior early in its history (*Wood et al.,* 1970), receded from Earth rapidly, before significant freezing out of the magma ocean likely occurred. Dynamical mechanisms that could slow the retreat of the Moon from Earth would cause significant heating of the lunar interior (*Touma and Wisdom,* 1994), and would exacerbate the problem of how to cool the Moon quickly enough to explain the degree-2 shape in the context of an earlier, faster rotation. Previous analysis of the compensation of long-wavelength loads (*Willemann and Turcotte,* 1981), and a more recent treatment of time-dependent load relaxation (*Zhong and Zuber,* 1999), show that compensation is strongly dependent on planetary radius, such that significant long wavelength loads can be supported over lunar history by a thin elastic lithosphere. However, current thermal models (e.g., *Pritchard and Stevenson,* 2000), which admittedly have significant uncertainties, favor hot early conditions. Joint consideration of dynamical and thermal models constrained by long wavelength topography and gravity will ultimately be required to resolve the inconsistency.

3. MANTLE COMPOSITION AND THERMAL STATE

The lunar mantle comprises about five-sixths of the lunar volume and therefore makes the main contribution to the Moon's bulk composition. To some extent, the composition of the upper mantle (60–500 km depth) can be inferred from surface mare basalt samples that experienced partial melting at depth and subsequent upward migration (e.g., *Ringwood and Essene,* 1970; *Delano,* 1986; *Taylor,* 1987). For example, a Mg number (Mg#) [molar MgO/(MgO + FeO) × 100] of the upper mantle in the range of 75–80 and a bulk Al_2O_3 content of <1 wt% may be estimated on this basis. However, few (if any) surface samples are believed to have originated in the middle and lower mantle (>500 km depth), representing more than one-third of the lunar volume. This region is therefore essentially inaccessible to direct or indirect chemical sampling and can only be characterized geophysically.

Geophysical constraints on the composition of the mantle come almost entirely from interpretations of seismic velocity models, supplemented by measurements of the lunar mean density and moment-of-inertia. As reviewed by *H86,* the small number (4) and areal distribution of the Apollo seismic stations combined with a low signal-to-noise ratio for lunar seismic signals has hindered accurate determinations of the seismic velocity structure of the mantle. A number of estimations of the velocity structure in the mantle were published based on early analyses of the Apollo seismic dataset (*Nakamura et al.,* 1976; *Goins,*

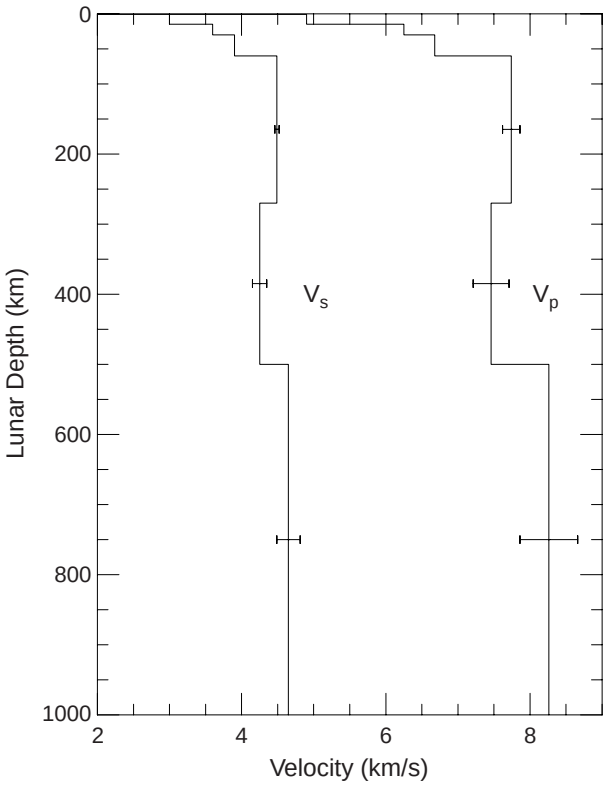

Fig. 3. P- and S-wave velocity model for the lunar mantle derived by *Nakamura* (1983). One-standard-deviation error limits resulting mainly from the variance in arrival time readings are shown.

1978; *Goins et al.*, 1981; *Nakamura*, 1983). Of these, the model of *Nakamura* (1983) (Fig. 3) is probably most accurate because it was the first to be based on the complete five-year Apollo record and analyzed signals from more deep moonquake sources (41) than had been considered previously. The Nakamura model is characterized by an apparent velocity decrease with depth in the upper mantle followed by a substantial velocity increase at ~500 km depth. As noted originally by *Nakamura* (1983), the 500-km velocity increase would imply either an increase in Mg# below this depth or a phase change, presumably involving the transition from the spinel to the garnet stability field for Al-bearing silicates.

Recently, *Khan* (1998) and *Khan et al.* (2000) have reported a new inversion of the complete Apollo seismic dataset using more modern, computationally intensive, inverse Monte Carlo methods. Only P-wave arrivals were analyzed, with results for the P-wave velocity structure shown in Fig. 4. Unlike the Nakamura model, the upper mantle velocity in the Khan model (8.1 ± 1.5 km/s) is essentially constant with increasing depth. Like the Nakamura model, the Khan model is characterized by a substantial velocity increase (to 9.0 ± 1.5 km/s) near 500 km. Moreover, as seen in Fig. 4, the velocity structure in the middle and lower mantle appears to be more inhomogeneous than in the upper mantle. In the deep moonquake source region, P-wave velocities are even larger (11.0 ± 1.2 km/s). Because of the more rigorous statistical technique, the Khan model represents an improvement over the Nakamura model. However, significant statistical uncertainties characterize both models and systematic errors (relating, for example, to lateral heterogeneities beneath the sparse Apollo seismic network) could well be present. In general, the middle and lower mantle P-wave velocities of the Khan model (9–11 km/s) are larger than those of the Nakamura model (8.26 ± 0.40 km/s) and the uncertainties are somewhat larger. In

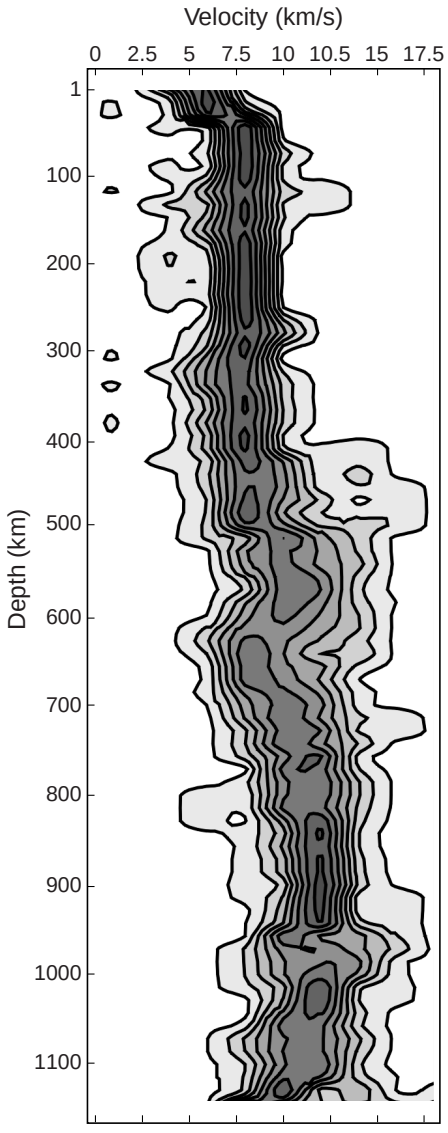

Fig. 4. P-wave seismic velocity model for the lunar mantle derived from the Apollo lunar seismic dataset by *Khan et al.* (2000) using an inverse Monte Carlo method. Contour lines define eight equal-spaced probability density intervals for the velocity distribution. The velocity increase near 500 km depth marks the transition from the upper mantle to the lower mantle. The deep moonquake source region is in the 850–960-km depth range. From *Khan et al.* (2000).

particular, it is possible that the more inhomogeneous middle mantle velocities may reflect, at least in part, a "leverage effect" due to data errors and/or model insensitivity at these depths.

Because of the significant temperature dependences of mineral elastic constants (see, e.g., *Hood and Jones,* 1987), quantitative interpretation of lunar seismic velocity models requires a prior consideration of bounds on the lunar mantle temperature profile. As reviewed, for example, by *H86*, constraints on the thermal structure of the lunar mantle come from surface heat flow data, seismic data, gravity data, and electromagnetic sounding data. At the surface, the mean temperature is measurable as ~0°C. At 300 km depth, a constraint on upper mantle temperatures of <800°C has been inferred from the apparent maintenance of mascon anisostasy over 3–4 eons (*Pullan and Lambeck,* 1980). This upper limit is consistent with the high mean seismic inverse dissipation (Q) values (4000–7000; *Nakamura and Koyama,*1982) in this depth range. In the middle mantle, Q-values are reduced to >1000, implying somewhat higher temperatures. However, the locations of most deep moonquake foci in the depth range from 850 to 960 km (*Khan et al.,* 2000) still requires temperatures well below the solidus at these depths to allow the implied accumulation of tidal stresses. At 850 km depth, the lunar solidus temperature may be estimated as 1400° ± 100°C, increasing to 1500° ± 100°C by 1000 km depth (*Ringwood and Essene,* 1970; *Hodges and Kushiro,* 1974). At depths greater than ~1000 km, S-wave Q-values decrease to ~100, implying greater dissipation and temperatures probably approaching the solidus. From the above constraints, a temperature profile that starts at 0°C at 0 km depth, increases to ~750°C at 300 km depth, to ~1200°C at 800 km depth, and to ~1400°C at 1100 km depth may be suggested. Such a profile is approximately consistent with some thermal history models (e.g., *Toksöz et al.,* 1978). The latter model assumed melting and differentiation to a depth of ~500 km and an average U concentration of 35 ppb. The model indicated that convective heat transport was important during early lunar history but is presently weak and confined mainly to the lower mantle.

As reviewed by *H86*, surface heat flow measurements were obtained at the Apollo 15 and 17 landing sites (21 and 16 mW/m^2 respectively) and have been applied to constrain both the thermal state and radioactive elemental composition of the lunar interior. By extrapolating these isolated measurements using orbital data on surface Th abundances and inferred crustal thicknesses, *Langseth et al.* (1976) originally estimated a global mean heat flow rate of 18 mW/m^2. Such a high mean heat flow value would imply bulk lunar U abundances ranging from 35 to 46 ppb, depending on whether secular cooling is important or whether a simple steady-state balance exists between heat production and loss respectively. These values are much larger than that for the bulk Earth (18 ppb) and would therefore support the view that the Moon is enriched in refractory elements (e.g., *Taylor,* 1987). However, *Rasmussen and Warren* (1985) later argued that the Apollo 15 and 17 landing sites were near the edges of maria where megaregolith thickness may be unusually shallow, leading to anomalously high heat flow rates. On this basis, they proposed an alternate global mean heat flow rate of 11 mW/m^2. Such a global mean value would imply bulk lunar U abundances ranging from 20 to 27 ppb. The lower limit of this range is not significantly different from the terrestrial value. They therefore argued that the Apollo heat flow data alone do not definitively require a lunar excess of refractory elements. It may be concluded from these results that additional direct lunar heat flow measurements in a wider variety of geologic settings are probably needed before a firm constraint on either lunar bulk composition or thermal state will be possible.

Several of the Apollo-era seismic models have been analyzed to infer constraints on the structure and composition of the lunar mantle (*Buck and Toksöz,* 1980; *Basaltic Volcanism Study Project,* 1981; *Hood and Jones,* 1987; *Mueller et al.,* 1988). Of most interest here are the studies by *Hood and Jones* (1987) and *Mueller et al.* (1988), who analyzed the later and more accurate *Nakamura* (1983) model. In the study by *Hood and Jones* (1987), forward calculations were performed of seismic velocity profiles for several possible lunar bulk compositions, differentiation schemes, and thermal gradients. Comparisons of the calculated profiles to the Nakamura model favored models that assumed differentiation of the upper mantle only, that were more aluminous in bulk composition than the terrestrial mantle, and that were characterized by an increase in Mg# in the middle and lower mantle relative to the upper mantle. Although seismic velocities tended to decrease in the upper mantle because of the large thermal gradient in this zone, the calculated decrease was generally too small to match that of the Nakamura model. (Note, however, that the Khan model has no significant velocity decrease in the upper mantle.) In the study by *Mueller et al.* (1988), an attempt was made to "invert" the Nakamura model to find the range of lunar compositional and evolutionary models consistent with the observational seismic velocities. These authors also inferred that an increase in aluminous phases and an increase in Mg# was probably required in the middle and lower mantle to explain the P-wave velocity increase at 500 km depth. They concluded that the 500-km discontinuity probably marks the lowest extent of lunar differentiation and may represent a transition to a less fractionated, possibly primordial middle and lower mantle.

Although the *Khan et al.* (2000) seismic model has not yet been quantitatively interpreted, the authors have noted several probable implications of the model for lunar structure and evolution. In particular, the nearly homogeneous upper mantle velocity structure and the more complex middle mantle structure were interpreted to imply early melting and differentiation to 500 km depth. Beneath this transition, the middle and lower mantle were suggested to consist of relatively "pristine" and inhomogeneous material. (Note again, however, that increased data errors and/or model insensitivity in the middle and lower mantle may

contribute to the more complex velocity structure at those depths.)

The above interpretations of the inferred seismic velocity structure of the lunar mantle have several interesting derivative implications for lunar origin and evolution models. In general, a preferred interpretation of the seismic velocity increase at 500 km depth is a change in composition to more aluminous, more MgO-rich mafic silicates. This inferred composition change, combined with the evidence for a homogeneous upper mantle and an inhomogeneous middle and lower mantle, is most easily understood if the Moon was initially melted and differentiated only to a depth of 500 km. Initial differentiation to 500 km means that all the Al now in the lunar crust must have been extracted from the upper mantle. This inference, combined with the increased alumina abundance in the middle and lower mantle, as well as petrologic evidence for a reduced Mg# in the lunar upper mantle, increases the likelihood that the Moon's bulk composition differs significantly from that of the terrestrial mantle. As noted by *Mueller et al.* (1988), this compositional dissimilarity is sufficient to dismiss classical fission models even without considering dynamical objections.

Of the remaining models for lunar origin (capture, binary accretion, impact-fission), the impact-fission model is currently considered to be the most dynamically plausible (e.g., *Cameron,* 1997; *Canup and Esposito,* 1996). As pointed out by *Mueller et al.* (1988), a primitive, undifferentiated middle and lower mantle consisting of more aluminous and MgO-rich phases could be consistent with such a model. Because the impactor mass and composition are poorly constrained, the initial composition of the impact-produced vapor cloud is not precisely known. However, MgO is more refractory than FeO under vapor conditions (*Grossman and Larimer,* 1974) and alumina is a very refractory component of a silicate vapor. It may therefore be suggested that fractional condensation of the impact vapor would favor a more aluminous and MgO-rich composition for the earliest condensates. As also noted by *Mueller et al.* (1988), these condensates may have accreted to form a small proto-Moon that could have remained unmelted because of smaller accretional energy deposition, larger surface area to volume ratio, and a relatively high melting temperature. Later addition of less refractory material at higher impact velocities may have melted only the outer 500 km of the final proto-Moon, producing the upper mantle and crust.

4. CORE

As reviewed in more detail by *H86*, independent geophysical constraints on the existence and size of a lunar metallic core come from gravity data, seismic data, electromagnetic sounding data, laser ranging data, and paleomagnetic data. Recent measurements by instruments on the Lunar Prospector spacecraft as well as continued ground-based laser ranging measurements have led to significant refinements of these constraints. Although none is individually definitive, as reviewed below, together they provide strong evidence for the existence of a small lunar metallic core representing 1–3% of the lunar mass.

One indirect approach toward investigating the existence of a dense metallic core is to apply the moment of inertia constraint together with thermal and density models of the lunar crust and mantle (*Hood and Jones,* 1987; *Mueller et al.,* 1988). During the post-Apollo period, the best available determination of the normalized polar moment of inertia was 0.3905 ± 0.0023 (*Ferrari et al.,* 1980). Adopting an upper bound of 0.3928, both *Hood and Jones* (1987) and *Mueller et al.* (1988) found that mantle density increases alone were insufficient to match this adopted limit for plausible thermal, compositional, and evolutionary models of the lunar interior. A small dense core was therefore suggested. Considering independent limits on the maximum core size from electromagnetic sounding data, *Hood and Jones* (1987) concluded that a core representing 1–4% of the lunar mass was most probable. Corresponding core radius limits are in the range of 200–450 km for an Fe composition. Recently, *Konopliv et al.* (1998) have reported a significantly improved determination of the normalized polar moment of 0.3932 ± 0.0002 using Lunar Prospector Doppler gravity data. The corresponding upper bound of 0.3934 is only marginally larger than that adopted previously by *Hood and Jones* (1987) and by *Mueller et al.* (1988). Their conclusions with respect to the existence of a small core remain unchanged. However, the more accurate and larger value of the normalized moment increases confidence that no more than a small core is present.

Ideally, by analogy with the terrestrial case, seismic arrival time data could be used to determine directly the existence and size of a metallic core since seismic velocities are significantly reduced in a metallic medium. However, the low signal-to-noise ratio of lunar seismic signals limited the efficacy of this approach in the case of the Apollo seismic dataset (*H86*). Future lunar seismic data may be acquired by the planned Japanese LUNAR-A penetrator mission (*Mizutani,* 1995). Three penetrators containing ultrasensitive seismometers and heat-flow probes will be emplaced at locations diametrically opposite to one another and to the known locations of deep moonquake sources. The mission is designed to exploit knowledge gained from the Apollo network in order to better investigate the existence and size of a metallic core.

A third approach toward investigating the existence and size of a metallic core takes advantage of the core's high electrical conductivity relative to that of the mantle. In addition to time-dependent electromagnetic induction studies that normally employ simultaneous data from at least two magnetometers (*H86*), an alternate approach toward core detection requires data from a single magnetometer in low-altitude lunar orbit (Fig. 5). In this approach, time intervals are identified when the Moon is exposed for prolonged periods to a nearly spatially uniform magnetic field in a near-vacuum environment. Conditions that approximate this idealized situation occur occasionally each month when the Moon passes through a lobe of the geomagnetic tail. Ex-

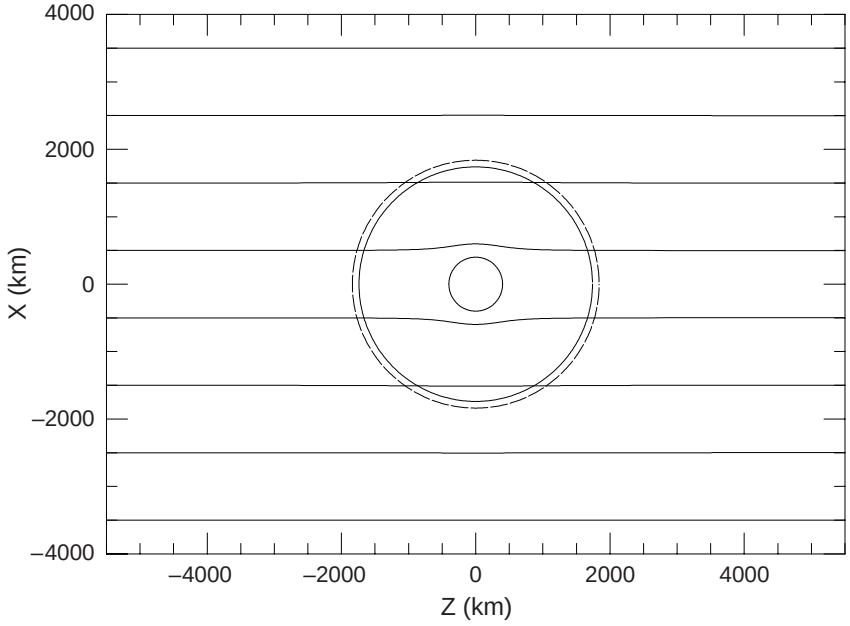

Fig. 5. Perturbation of spatially uniform magnetic field lines by an induced magnetic field caused by currents at the surface of a highly electrically conducting core of radius 400 km (inner circle). The outer solid circle represents the projection of the lunar surface and the outermost dashed circle indicates a nominal Lunar Prospector orbit at 100 km altitude. The orbit plane is parallel to the applied field orientation. From *Hood et al.* (1999).

posure of the Moon to such a steady field induces electrical currents in the lunar interior with an associated negative induced magnetic dipole moment oriented opposite to the applied field. The sum of the steady field and the induced field produces a perturbation as shown in Fig. 5. After currents in the lunar mantle have decayed (~5 h or less), any residual steady induced moment is expected to be due to currents near the surface of a possible highly electrically conducting core. The amplitude of the residual moment is then relatable to the core radius.

Measurements of the lunar induced moment in the geomagnetic tail were originally obtained using data from magnetometers on the Apollo 15 and 16 subsatellites (*Russell et al.*, 1981). Careful editing to eliminate periods when significant plasma densities were present resulted in a final estimated induced moment of $-4.23 \pm 0.64 \times 10^{22}$ Gauss-cm^3 per Gauss of applied field. Assuming that this moment was entirely caused by a metallic core, the core radius was estimated as 439 ± 22 km. As discussed by *H86*, possible error sources include paramagnetic effects (mean permeability >1) and incomplete decay of mantle-induced fields resulting from short-term changes in the mean field amplitude.

Since the launch of Lunar Prospector in January 1998, an effort has been made to obtain independent measurements of the lunar induced moment in the geomagnetic tail (*Hood et al.*, 1999). Because Lunar Prospector is in a near-polar orbit, measurements of the induced moment are geometrically most feasible when the orbit plane is nearly parallel to the Sun-Moon line (parallel to the Z axis in Fig. 5). This occurs approximately at six-month intervals. The first opportunity for optimal measurements, i.e., the first period when the orbit plane was optimally aligned, occurred in April 1998. During this month, the Moon fortuitously entered the north tail lobe and remained there for an unusually long period (>2 days) during which the tail lobe field was relatively strong and steady. Careful editing and averaging of individual orbit segments increased the signal-to-noise ratio and allowed a measurement of the induced moment as $-2.4 \pm 1.6 \times 10^{22}$ Gauss-cm^3 per Gauss of applied field. Figure 6 plots the variance between the mean observed field perturbation and that expected theoretically as a function of core size. It is seen that the data strongly exclude cores with radii larger than 450 km, but cores smaller than 300 km radius are less strongly excluded. The preferred moment amplitude is slightly smaller than that obtained by *Russell et al.* (1981), but the two estimates are marginally consistent within the 1σ uncertainties of the measurements. Assuming that the induced field is caused

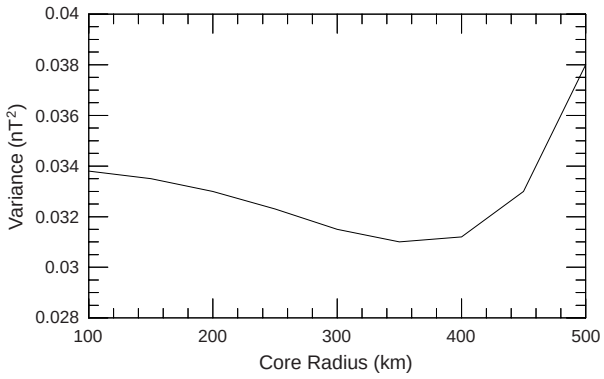

Fig. 6. Variances of model field perturbations from observed mean field perturbations as a function of induced moment amplitude. Equivalent core radii are also indicated on the lower scale. From *Hood et al.* (1999).

entirely by electrical currents near the surface of a highly electrically conducting metallic core, the preferred core radius is 340 ± 90 km, representing 1–3% of the lunar mass. However, when uncertainties related to the possible presence of residual mantle-induced fields are considered, this measurement should be regarded as an upper limit on the core radius (430 km at the 1σ level).

One additional property of a metallic core that may be detectable geophysically is its liquid state. Thermal history models (e.g., *Konrad and Spohn,* 1998) indicate that Fe cores containing a small amount of S can remain liquid through the entire 4.6 b.y. of lunar evolution. A fluid metallic core enhances friction at the core-mantle boundary, causing a larger dissipation of rotational energy in the Moon than would be expected without a fluid core (*Yoder,* 1981, 1984; *Ferrari et al.,* 1980). Lunar laser ranging measurements of physical libration parameters have shown that the lunar rotation axis is advanced by about 0.2 arcsec from the Cassini alignment, indicating significant internal dissipation. In addition to solid-state friction in the lunar mantle, friction at the boundary between a fluid core and a solid silicate mantle appears to be necessary to explain the magnitude of this advance. On the basis of a turbulent coupling model, *Yoder* (1981) originally inferred a probable core radius of 330 km. More recently, additional laser ranging data and an improved gravity field from Lunar Prospector Doppler tracking have allowed a reevaluation of this constraint on the existence and size of a fluid lunar core. Taking into account all uncertainties, including possible topography on the core-mantle boundary as well as theoretical uncertainties, a 1σ upper limit of 352 km on the core radius for an assumed Fe composition has been reported (*Williams et al.,* 1999). For an Fe-FeS eutectic composition, the upper limit is increased to 374 km. It should be noted that an additional solid inner core is neither excluded nor required by the available ranging data.

Finally, one additional geophysical indication of the possible existence of a lunar metallic core is the observed pervasive paleomagnetism of lunar crustal materials (for reviews, see *Fuller,* 1974; *Fuller and Cisowski,* 1987; *Hood,* 1995). Paleointensity estimates for returned lunar samples suggest relatively large (~1 Gauss) surface magnetizing fields between about 3.6 and 3.8 eons b.p. (*Cisowski et al.,* 1983; *Cisowski and Fuller,* 1986). This would be suggestive of a former core dynamo. On the other hand, orbital measurements indicate an important role for impact processes in producing the strongest concentrations of crustal magnetic anomalies. First, low-altitude passes across the lunar nearside by the Apollo 16 subsatellite magnetometer showed that fields are relatively weak across the maria but are larger over exposures of the Fra Mauro and Cayley Formations (primary and secondary basin ejecta respectively) (*Hood et al.,* 1979). It had previously been shown from sample studies that mare basalts contain relatively little microscopic Fe remanence carriers, while impact-produced breccias and soils contain much more of these carriers (*Strangway et al.,* 1973). Thus the absence of strong fields over the maria as compared to the highlands and impact basin ejecta could be understood since impact processes played an important role in producing larger concentrations of remanence carriers. Second, the four largest concentrations of magnetic anomalies within the region mapped by the Apollo subsatellites occurred near the antipodes of the four youngest and largest impact basins: Imbrium, Orientale, Serenitatis, and Crisium (*Lin et al.,* 1988). More recent mapping using improved data coverage by the Lunar Prospector magnetometer and electron reflectometer has confirmed this correlation (*Lin et al.,* 1998). A model for the origin of magnetic anomalies antipodal to lunar impact basins involving expansion of a massive, partially ionized impact vapor cloud around the Moon has been partially developed (*Hood and Huang,* 1991). Nevertheless, the origin of the ambient magnetic field remains unclear. A core dynamo origin cannot be excluded by the orbital data alone since impact processes have greatly complicated the distribution and orientation of crustal anomaly sources. On the other hand, a core dynamo is also not required to be present according to some impact field models (e.g., *Hood and Huang,* 1991).

In summary, gravity, electromagnetic sounding, and laser ranging data appear to be converging in indicating the existence of a small dense, highly electrically conducting, and probably fluid core within the Moon. The most probable core radius is in the range of 300–400 km, representing ~1–3% of the lunar mass. However, when all uncertainties are considered, both the laser ranging data and the electromagnetic sounding data are most conservatively interpreted as implying only an upper limit on the core radius, 352 km in the case of the ranging data and 430 km in the case of the induced moment measurements. Likewise, uncertainties in mantle thermal, composition, and evolutionary models as constrained by seismic velocity models are sufficiently large that the existence of a dense core is only marginally indicated (*Mueller et al.,* 1988). Consequently, although the existence of a metallic core is the most probable interpretation of the available data, additional measurements (possibly those planned for the Japanese LUNAR-A mission) are needed to more definitively resolve this fundamental issue.

5. SUMMARY

As discussed in section 2, Clementine and Lunar Prospector gravity and topography data demonstrate a wide range of global crustal thickness variations (~20–110 km), implying either impact-related redistribution of crustal materials or lateral heterogeneities in early melting and differentiation, or both. The mean crustal thickness is ~61 km with larger mean values on the farside except beneath the South Pole-Aitken Basin. Recent modeling of mascon gravity anomalies supports the view that they are caused by a combination of postimpact rebound of the crust followed by mare filling. Support for this view comes from observations of mascons associated with several farside basins

that appear to lack mare fill. Modeling of regional and long-wavelength Clementine and Lunar Prospector data provide evidence for a rigid lunar lithosphere well before the mare emplacement epoch. The observed topographic flattening of the Moon and the ellipticity of the lunar equator appear to imply that the Moon was unexpectedly close (13–16 R_E) to the Earth when its present shape was "frozen in." Such rapid early cooling to produce the significant degree-2 power in the lunar shape is contrary to expectations from dynamical models of the evolution of the Earth-Moon system, as well as thermal models of the early lunar thermal state. Resolution of the inconsistency will require coupled dynamical and thermal models constrained by topography and gravity.

As reviewed in section 3, quantitative compositional modeling of the *Nakamura* (1983) seismic velocity model strongly suggests that initial melting and differentiation of the lunar interior was confined to the upper mantle (<500 km depth). An increase in alumina abundance and in MgO content is also probably needed in the middle and lower mantle. If differentiation was limited to 500 km depth, it becomes difficult to explain the alumina abundance in the crust unless the initial alumina content in the upper mantle was enriched relative to that of the terrestrial mantle. The recent *Khan et al.* (2000) P-wave velocity model is most consistent with a compositionally homogeneous upper mantle and a much more heterogeneous middle mantle. These results also independently suggest initial melting and differentiation of the upper mantle only. As also discussed in section 3, *Mueller et al.* (1988) specifically argue that the middle and lower mantle may represent a primordial, unmelted, refractory-rich basement on which less refractory material accreted and subsequently melted. Such an interpretation could, in principle, be consistent with fractional condensation of a vapor cloud produced according to the giant impact model, for example. A primitive, unmelted deep interior would require that any metallic core have formed via heterogeneous accretion or incremental separation of more mobile metallic phases accompanying partial melting events (without melting and homogenizing the entire proto-Moon). As reviewed by *Pritchard and Stevenson* (2000), the giant impact model does not yet accurately predict the precise thermal state of the proto-Moon because of a poor understanding of the dynamical continuum disk phase that immediately follows the impact event.

As reviewed in section 4, quantitative assessments of all available geophysical constraints, including the moment of inertia, suggest the presence of a small dense core with a mass exceeding ~1% of the lunar mass. Recent analyses of Lunar Prospector magnetometer data, gravity data, and groundbased laser ranging data independently suggest the presence of a metallic core with a radius in the range of 300–400 km. However, in the most conservative interpretation, only an upper bound on the core radius is implied by both the magnetometer data and the laser ranging data. Thus, future measurements [such as those to be obtained during the planned LUNAR-A mission (*Mizutani,* 1995)] may be needed to more definitively establish the existence of a metallic core.

Acknowledgments. Thanks are due to A. Konopliv, G. Neumann, D. Smith, and M. Wieczorek for contributing data and models presented herein. A. Khan kindly provided a copy of Fig. 4 in advance of publication. Finally, we thank Kevin Righter for the initial invitation to write this chapter and Roger Phillips for a constructive, critical review.

Note added in proof: Further analysis of Apollo seismic data, including S-wave data as well as P-wave data, yields a revised estimate for the maximum depth of the upper mantle as 550 ± 20 km (A. Khan personal communication, 1999).

REFERENCES

Basaltic Volcanism Study Project (1981) *Basaltic Volcanism on the Terrestrial Planets.* Pergamon, New York. 1286 pp.

Bills B. G. and Ferrari A. J. (1977) A harmonic analysis of lunar topography. *Icarus, 31,* 244–259.

Bills B. G. and Ferrari A. J. (1980) A harmonic analysis of lunar gravity. *J. Geophys. Res., 85,* 1013–1025.

Binder A. B., Feldman W. C., Hubbard G. S., Konopliv A., Lin R. P., Acuna M. A., and Hood L. L. (1998) Lunar Prospector searches for polar ice, a metallic core, gas release events, and the Moon's origin. *Eos Trans. AGU, 79,* 97–108.

Bratt S. R., Solomon S. C., Head J. W., and Thurber C. H. (1985) The deep structure of lunar basins: Implications for basin formation and modification. *J. Geophys. Res., 90,* 3049–3064.

Brown W. E. Jr., Adams G. F., Eggleton R. E., Jackson P., Jordan R., Kobrick M., Peeples W. J., Phillips R. J., Porcello L. J., Schaber G., Sill W. R., Thompson T. W., Ward S. H., and Zelenka J. S. (1974) Elevation profiles of the Moon. *Proc. Lunar Sci. Conf. 5th,* pp. 3037–3048.

Budney C. J. and Lucey P. G. (1998) Basalt thickness in Mare Humorum: The crater excavation method. *J. Geophys. Res., 103,* 16855–16870.

Buck W. R. and Toksöz M. N. (1980) The bulk composition of the Moon based on geophysical constraints. *Proc. Lunar Planet. Sci. Conf. 11th,* pp. 2043–2058.

Cameron A. G. W. (1997) The origin of the Moon and the single impact hypothesis V. *Icarus, 126,* 126–137.

Canup R. M. and Esposito L. W. (1996) Accretion of the Moon from an impact-generated disk. *Icarus, 119,* 427–446.

Cisowski S. M. and Fuller M. (1986) Lunar paleointensities via the IRMs normalization method and the early magnetic history of the Moon. In *Origin of the Moon* (W. K. Hartmann, R. J. Phillips, and G. J. Taylor, eds.), pp. 411–424. Lunar and Planetary Institute, Houston.

Cisowski S. M., Collinson D. W., Runcorn S. K., Stephenson A., and Fuller M. (1983) A review of lunar paleointensity data and implications for the origin of lunar magnetism. *Proc. Lunar Planet. Sci. Conf. 13th,* in *J. Geophys. Res., 88,* A691–A704.

Comer R. P., Solomon S. C., and Head J. W. (1979) Elastic lithosphere thickness on the Moon from mare tectonic features: A formal inversion. *Proc. Lunar Planet. Sci. Conf. 10th,* pp. 2441–2463.

Delano J. W. (1986) Abundances of cobalt, nickel, and volatiles in the silicate portion of the Moon. In *Origin of the Moon* (W. K. Hartmann, R. J. Phillips, G. J. Taylor, eds.), pp. 231–247. Lunar and Planetary Institute, Houston.

Ferrari A. J., Sinclair W. S., Sjogren W. L., Williams J. G., and Yoder C. F. (1980) Geophysical parameters of the Earth-Moon system. *J. Geophys. Res., 85,* 3939–3951.

Fuller M. (1974) Lunar magnetism. *Rev. Geophys. Space Phys., 12,* 23–70.

Fuller M. and Cisowski S. (1987) Lunar paleomagnetism. In *Geomagnetism* (J. A. Jacobs, ed.), pp. 307–456.

Goins N. R. (1978) The internal structure of the Moon. Ph.D. thesis, Massachusetts Institute of Technology, Cambridge. 666 pp.

Goins N. R., Dainty A. M., and Toksöz M. N. (1981) Lunar seismology: The internal structure of the Moon. *J. Geophys. Res., 86,* 5061–5074.

Goldreich P. (1966) History of the lunar orbit. *Rev. Geophys., 4,* 411–439.

Grossman L. and Larimer J. W. (1974) Early chemical history of the solar system. *Rev. Geophys., 12,* 71–101.

Hodges F. N. and Kushiro I. (1974) Apollo 17 petrology and experimental determination of differentiation sequences in model Moon compositions. *Proc. Lunar Sci. Conf. 5th,* pp. 505–520.

Hood L. L. (1986) Geophysical constraints on the lunar interior. In *Origin of the Moon* (W. K. Hartmann, R. J. Phillips, and G. J. Taylor, eds.), pp. 361–410. Lunar and Planetary Institute, Houston.

Hood L. L. (1995) Frozen fields. *Earth, Moon, and Planets, 67,* 131–142.

Hood L. L. and Huang Z. (1991) Formation of magnetic anomalies antipodal to lunar impact basins: Two-dimensional model calculations. *J. Geophys. Res., 96,* 9837–9846.

Hood L. L. and Jones J. (1987) Geophysical constraints on lunar bulk composition and structure: A reassessment. *Proc. Lunar Planet. Sci. 17th,* in *J. Geophys. Res., 92,* E396–E410.

Hood L. L., Coleman P. J. Jr., and Wilhelms D. E. (1979) The Moon: Sources of the crustal magnetic anomalies. *Science, 204,* 53–57.

Hood L. L., Lin R. P., Mitchell D. L., Acuna M. H., and Binder A. B. (1999) Initial measurements of the lunar induced magnetic moment in the geomagnetic tail using Lunar Prospector data (abstract). In *Lunar and Planetary Science XXX,* Lunar and Planetary Institute, Houston.

Jeffreys H. (1970) *The Earth.* Cambridge Univ., New York. 525 pp.

Kaula W. L., Schubert G., Lingenfelter R. E., Sjogren W. L., and Wollenhaupt W. R. (1974) Apollo laser altimetry and inferences as to lunar surface structure. *Proc. Lunar Sci. Conf. 5th,* pp. 3049–3058.

Khan A. (1998) A selenological enquiry. M.S. thesis, Odense University. 99 pp.

Khan A., Mosegaard K., and Rasmussen K. L. (2000) Seismic evidence for a lunar magma ocean extending to 560 km depth. *Geophys. Res. Lett.,* submitted.

Konopliv A. S., Sjogren W. L., Wimberly R. N., Cook R. A., and Vijayaraghavan A. (1993) A high-resolution lunar gravity field and predicted orbit behavior. AAS Paper 93-622, AAS/AIAA Astrodynamics Specialist Conference, Victoria, British Columbia.

Konopliv A. S., Binder A., Hood L., Kucinskas A., Sjogren W. L., and Williams J. G. (1998) Gravity field of the Moon from Lunar Prospector. *Science, 281,* 1476–1480.

Konrad W. and Spohn T. (1998) The influence of lunar mantle convection on partial melting and the cooling of a small core (abstract). In *Origin of the Earth and Moon,* pp. 20–21. LPI Contrib. No. 957, Lunar and Planetary Institute, Houston.

Lambeck K. and Pullan S. (1980) The lunar fossil bulge hypothesis revisited. *Phys. Earth Planet. Inter., 22,* 29–35.

Langseth M. G., Keihm S. J., and Peters K. (1976) Revised lunar heat flow values. *Proc. Lunar Sci. Conf. 7th,* pp. 3143–3171.

Lemoine F. G., Smith D. E., Zuber M. T., Neumann G. A., and Rowlands D. D. (1997) A 70th degree lunar gravity model from Clementine and other tracking data. *J. Geophys. Res., 102,* 16339–16359.

Lin R. P., Anderson K. A., and Hood L. L. (1988) Lunar surface magnetic field concentrations antipodal to young large impact basins. *Icarus, 74,* 529–541.

Lin R. P., Mitchell D. L., Curtis D. W., Anderson K. A., Carlson C. W., McFadden J., Acuña M., Hood L., and Binder A. (1998) Lunar surface magnetic fields and their interaction with the solar wind: Results from Lunar Prospector. *Science, 281,* 1480–1484.

Lucey P. G., Spudis P. D., Zuber M., Smith D., and Malaret E. (1994) Topographic-compositional units on the Moon and the early composition of the lunar crust. *Science, 266,* 1855–1858.

Lucey P. G., Taylor G., Hawke B. R., and Spudis P. D. (1998) FeO and TiO_2 concentrations in the South Pole-Aitken basin: Implications for mantle composition and basin formation. *J. Geophys. Res., 103,* 3701–3708.

Melosh H. J. (1989) *Impact Cratering: A Geologic Process.* Oxford Univ., New York, 245 pp.

Mizutani H. (1995) Lunar interior exploration by Japanese lunar penetrator mission, LUNAR-A. *J. Phys. Earth, 43,* 657–670.

Mueller S., Taylor G. J., and Phillips R. J. (1988) Lunar composition: A geophysical and petrological synthesis. *J. Geophys. Res., 93,* 6338–6352.

Muller P. M. and Sjogren W. L. (1968) Mascons: Lunar mass concentrations. *Science, 161,* 680–684.

Nakamura Y. (1983) Seismic velocity structure of the lunar upper mantle. *J. Geophys. Res., 88,* 677–686.

Nakamura Y. and Koyama J. (1982) Seismic Q of the lunar upper mantle. *J. Geophys. Res., 87,* 4855–4861.

Nakamura Y., Duennebier F., Latham G., and Dorman H. (1976) Structure of the lunar mantle. *J. Geophys. Res., 81,* 4818–4824.

Neumann G. A., Zuber M. T., Smith D. E., and Lemoine F. G. (1996) The lunar crust: Global signature and structure of major basins. *J. Geophys. Res., 101,* 16,841–16,863.

Nozette S., Rustan P. L., Plesance L. P., Horan D. M., Regeon P., Shoemaker E. M., Spudis P. D., Acton C., Baker D. N., Blamont J. E., Buratti B. J., Corson M. P., Davies M. E., Duxbury T. C., Eliason E. M., Jakosky B. M., Kordas J. F., Lewis I. T., Lichtenberg C. L., Lucey P. G., Malaret E., Massie M. A., Resnick J. H., Rollins C. J., Park H. S., McEwen A. S., Priest R. E., Pieters C. M., Reisse R. A., Robinson M. S., Simpson R. A., Smith D. E., Sorenson T. C., Vorder Bruegge R. W., and Zuber M. T. (1994) The Clementine mission to the Moon: Scientific overview. *Science, 266,* 1835–1839.

Phillips R. J. and Dvorak J. (1981) The origin of lunar mascon basins: Analysis of the Bouguer gravity associated with Grimaldi. In *Multi-Ring Basins, Proc. Lunar Planet. Sci. 12A* (P. H. Schultz and R. B. Merrill, eds.), pp. 91–104.

Phillips R. J., Sjogren W. L., Abbott E. A., and Zisk S. H. (1978) Simulation gravity modeling to spacecraft tracking data: Analysis and application. *J. Geophys. Res., 83,* 5455–5464.

Pritchard M. E. and Stevenson D. J. (2000) Thermal aspects of a lunar origin by giant impact. In *Origin of the Earth and Moon* (R. M. Canup and K. Righter, eds.), this volume. Univ. of Arizona, Tucson.

Pullan S. and Lambeck K. (1980) On constraining lunar mantle

temperatures from gravity data *Proc. Lunar Planet. Sci. Conf. 11th*, pp. 2031–2041.

Rasmussen K. L. and Warren P. H. (1985) Megaregolith thickness, heat flow, and the bulk composition of the Moon. *Nature, 313*, 121–124.

Ringwood A. E. and Essene E. (1970) Petrogenesis of Apollo 11 basalts, internal constitution and origin of the Moon. *Proc. Apollo 11 Lunar Sci. Conf.*, pp. 769–799.

Russell C. T., Coleman P. J. Jr., and Goldstein B. E. (1981) Measurements of the lunar induced magnetic moment in the geomagnetic tail: Evidence for a lunar core. *Proc. Lunar Planet. Sci. 12B*, pp. 831–836.

Smith D. E. and Zuber M. T. (1998) Inferences about the early Moon from gravity and topography (abstract). In *Origin of the Earth and Moon*, pp. 56–57. LPI Contribution No. 957, Lunar and Planetary Institute, Houston.

Smith D. E., Zuber M. T., Neumann G. A., and Lemoine F. G. (1997) Topography of the Moon from the Clementine LIDAR. *J. Geophys. Res., 102*, 1591–1611.

Smith D. E., Tyler G. L., Balmino G., and Sjogren S. L. (1999) The gravity field of Mars from Mars Global Surveyor. *Science*, submitted.

Solomon S. C. (1978) The nature of isostasy on the Moon: How big a Pratt-fall for Airy models? *Proc. Lunar Planet. Sci. Conf. 9th*, pp. 3499–3511.

Solomon S. C. (1986) On the early thermal state of the Moon. In *Origin of the Moon* (W. K. Hartmann, R. J. Phillips, and G. J. Taylor, eds.), pp. 435–452. Lunar and Planetary Institute, Houston.

Solomon S. C. and Head J. W. (1980) Lunar mascon basins: Lava filling, tectonics and evolution of the lithosphere. *Rev. Geophys., 18*, 107–141.

Solomon S. C. and Simons M. (1996) The isostatic state of the lunar highlands from spatio-spectral localization of gravity, topography, and surface chemistry (abstract). In *Lunar and Planetary Science XXVII*, pp. 1245–1246.

Strangway D. W., Sharpe H., Gose W., and Pearce G. (1973) Magnetism and the history of the Moon. In *Magnetism and Magnetic Materials — 1972* (C. D. Graham Jr. and J. J. Rhyne, eds.), pp. 1178–1187. American Institute of Physics, New York.

Taylor S. R. (1987) The unique lunar composition and its bearing on the origin of the Moon. *Geochim. Cosmochim. Acta, 51*, 1297–1309.

Thurber C. H. and Solomon S. C. (1978) An assessment of crustal thickness variations on the lunar nearside: Models, uncertainties, and implications for crustal differentiation. *Proc. Lunar Planet. Sci. Conf. 9th*, 3481–3497.

Toksöz M. N., Hsui A. T., and Johnston D. H. (1978) Thermal evolutions of the terrestrial planets. *Moon and Planets, 18*, 281–320.

Touma J. (2000) The phase space adventure of Earth and Moon. In *Origin of the Earth and Moon* (R. M. Canup and K. Righter, eds.), this volume. Univ. of Arizona, Tucson.

Touma J. and Wisdom J. (1994) Evolution of the Earth-Moon system. *Astron. J., 108*, 1943–1961.

von Frese R. R. B., Tan L., Potts L. V., Merry C. J., and Bossler J. D. (1996) Lunar crustal analysis of Mare Orientale from Clementine satellite observations. *J. Geophys. Res., 102*, 25657–25676.

Wieczorek M. A. and Phillips R. J. (1997) The structure and compensation of the lunar highland crust. *J. Geophys. Res., 102*, 10933–10943.

Wieczorek M. A. and Phillips R. J. (1998) Potential anomalies on a sphere: Applications to the thickness of the lunar crust. *J. Geophys. Res., 103*, 1715–1724.

Willemann R. J. and Turcotte D. L. (1981) Support of topographic and other loads on the Moon and on the terrestrial planets. *Proc. Lunar Planet. Sci. 12B*, pp. 837–851.

Williams J. G., Boggs D. H., Ratcliff J. T., and Dickey J. O. (1999) The Moon's molten core and tidal Q (abstract). In *Lunar and Planetary Science XXX*, Lunar and Planetary Institute, Houston.

Williams K. K. and Zuber M. T. (1998) Measurement and analysis of major lunar basin depths from Clementine altimetry. *Icarus, 131*, 107–122.

Wise D. U. and Yates M. Y. (1970) Lunar anorthosites and a geophysical model for the Moon. (1970) *Proc. Apollo 11 Lunar Sci. Conf.*, pp. 958–988.

Wood J. A., Dickey J. S. Jr., Marvin U. B., Powell B. N., and Yates M. Y. (1970) Mascons as subsurface relief on a lunar "Moho". *J. Geophys. Res., 75*, 261–268.

Yoder C. F. (1981) The free librations of a dissipative Moon. *Philos. Trans. Roy. Soc. London, A303*, 327–338.

Yoder C. F. (1984) The size of the lunar core (abstract). In *Papers Presented to the Conference on the Origin of the Moon*, p. 6. Lunar and Planetary Institute, Houston.

Zhong S. and Zuber M. T. (1999) Long-wavelength topographic relaxation for self-gravitating planets and implications for the time-dependent compensation of surface topography. *J. Geophys. Res.*, submitted.

Zuber M. T., Smith D. E., Lemoine F. G., and Neumann G. A. (1994) The shape and internal structure of the Moon from the Clementine mission. *Science, 266*, 1839–1843.